Turbulence-inclusive modelling of electron cyclotron wave-plasma dynamics in tokamaks

E. Devlaminck[1], J. Decker[1], S. Coda[1], L. Porte[1], J. Cazabonne[2], O. Maj[3], E. Poli[3], L. Votta[4], Y. Peysson[2] and the TCV team[1,a]

[1] *Ecole Polytechnique Fédérale de Lausanne (EPFL), Swiss Plasma Center (SPC), 1015 Lausanne, Switzerland*
[2] *Commissariat à l'Énergie Atomique et aux Énergies Alternatives (CEA), Institut de Recherche sur la Fusion par confinement Magnétique (IRFM), Cadarche, France*
[3] *Max Planck Institute for Plasma Physics, Garching, Germany*
[4] *KTH Royal Institute of Technology, Stockholm, Sweden*
[a] *See B.P. Duval et al 2024 Nucl. Fusion 64 112023.*

Introduction

Electron-cyclotron (EC) waves are widely used for plasma heating (ECH) and current drive (ECCD) in tokamaks. In addition to these main applications, the possibility of steering the launchers, together with a very localised power and current deposition, renders them appealing for instability mitigation as well as tailored control of current and pressure profiles. Owing to these attractive qualities, EC waves are envisioned as the main heating source for the ITER project [1]. However, previous work [2, 3] indicates that Fokker-Planck (FP) simulations coupled to a ray tracing code tend to overestimate the method's efficacy significantly when turbulent effects are overlooked. A significant numerical radial transport of suprathermal electrons (on the order of 1-4 m^2/s) has to be introduced ad-hoc, in order for the total plasma current and hard X-ray Bremsstrahlung predictions to reasonably agree with measurements on the *Tokamak à Configuration Variable* (TCV) [3]. The discrepancy with experimental results is believed to stem mainly from two effects, both of which find their origin in turbulence [4]: microwave beam broadening due to turbulent plasma density fluctuations and wave-enhanced turbulent transport of suprathermal electrons.

In this work, the goal was to couple two codes, *WKBeam* [5] and *LUKE* [6], to consistently simulate both of the aforementioned effects simultaneously for the first time. *WKBeam* solves the wave-kinetic equation (WKE) for the propagation of EC waves under the influence of time-averaged density fluctuations, while LUKE solves the linearised electron FP equation, considering the quasilinear wave-plasma interaction and allowing for ad-hoc radial transport of suprathermal electrons. The computation of the bounce-averaged quasilinear diffusion operator for radiofrequency waves from *WKBeam*, which is the key link in coupling both codes, is discussed in the following section.

The code suite is completed by synthetic diagnostic modules R5X2 [7] and YODA [8] for the Hard X-Ray Spectrometer (HXRS) and Vertical Electron Cyclotron Emission diagnostic (VECE) on TCV, respectively. An application of the full workflow, including this multidiagnostic approach to simulation optimisation, is covered in the third section.

The quasilinear diffusion operator

The incorporation of radiofrequency wave physics into a FP or drift-kinetic code like *LUKE* is mediated by a purely diffusive flux operator in spherical momentum coordinates ($p, \xi \triangleq p_\parallel/p$) [9]:

$$\mathbf{S}^{\mathrm{RF}} = -\mathbb{D}^{\mathrm{RF}} \cdot \nabla_{\mathbf{p}} f, \quad \text{with} \quad \mathbb{D}^{\mathrm{RF}} = \begin{pmatrix} D^{\mathrm{RF}}_{pp} & D^{\mathrm{RF}}_{p\xi} \\ D^{\mathrm{RF}}_{\xi p} & D^{\mathrm{RF}}_{\xi\xi} \end{pmatrix} \tag{1}$$

After bounce averaging (represented hereafter by $\langle\cdot\rangle$), each of the the tensor components in (1) can be readily calculated as linear combinations of the following form:

$$\langle D^{\mathrm{RF}}_{\alpha,\beta}\rangle(\psi, p, \xi_0) = \sum_{n=-\infty}^{+\infty} \sum_b \mathrm{A}_{\alpha,\beta}(\psi, \xi_0, b, n)\, \langle D^{\mathrm{RF}}_{b,n}\rangle\,(\psi, p, \xi_0) \tag{2}$$

where n is the harmonic number and the sum over b covers all beams of different frequencies. The calculation of the quasilinear diffusion coefficient $D^{\mathrm{RF}}_{b,n}$ and subsequent bounce averaging over

particle orbits (details of which can be found in [9]) from a *WKBeam* result is hence all that is needed to couple both codes. In the context of this work, $D^{\mathrm{RF}}_{b,n}$ can be conveniently rewritten as

$$D^{RF}_{n,b}(\psi,\theta,p,\xi) = \frac{1}{dV(\psi)}\frac{2\pi e^2}{|v_\parallel|\epsilon_0}\frac{c}{\omega_b}\int dN_\perp N_\perp \int dN_\parallel |\Theta^{bn}_{\mathbf{N}}|^2 \delta(N_\parallel - N_{\parallel res}) \int d\phi_N \mathcal{E}_N \quad (3)$$

where the integral over angular wavenumber space and the EC resonance condition have been reformulated in terms of the normalised refractive index N, with

$$N_{\parallel,res} \triangleq \frac{m_e c}{p\xi}\left(\gamma - \frac{n\omega_{ce}}{\omega_b}\right) \quad (4)$$

In (3), $dV(\psi)$ is the infinitesimal volume corresponding to a given flux surface, and $\mathcal{E}_N$ is the N-space energy density of the wave at the prescribed spatial location (ψ,θ). The expression for the polarisation term $|\Theta^{bn}_{\mathbf{N}}|^2$ in terms of Bessel functions is beyond the scope of this proceeding, and can be found in many standard works on quasilinear theory [10, 11].

In *WKBeam*, the WKE is solved for the *Wigner function* Ω under the influence of diffraction, linear absorption and scattering through density fluctuations. Ω can then be binned over arbitrarily defined bounds in $(\boldsymbol{x},\boldsymbol{N})$-space to give the electric field energy within each phase space volume. This way, $\int d\phi_N \mathcal{E}_N(\psi,\theta,N_\perp,N_\parallel)$ is readily computed and directly inserted into (3). A strongly optimised and parallelised module for the calculation of $\langle \mathbb{D}^{\mathrm{RF}} \rangle$ has been implemented into *WKBeam* for the purpose of this work.

Figure 1 shows the result of such a calculation without fluctuations at given ψ, as compared to the well-benchmarked ray tracing code *C3PO* [12], which is integrated in *LUKE*. The agreement in both phase space dependence and amplitude is excellent, and deviations can be attributed to the ray tracing-related approximations made in *C3PO*.

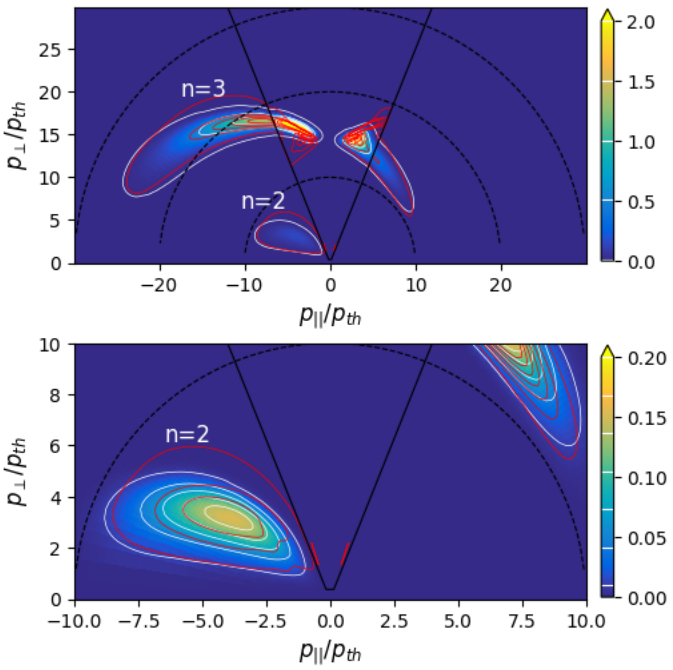

Fig. 1 *Top*: $\langle D^{\mathrm{RF}}_{b,n} \rangle$ at ψ_{abs}, computed based on a *WKBeam* simulation without density fluctuations (*background and white contours*). The result as obtained from *C3PO* is shown at the same contour values (*red*). *Bottom*: Zoom of the top plot to highlight the second harmonic, with adjusted colour and contour levels.

A multidiagnostic approach: TCV ECCD example

In this section, we present results from an application of the *LUKE-WKBeam* framework. TCV shot 86148 represents a 'worst-case' scenario for beam broadening achievable under ECCD conditions on the device. This discharge was carried out as part of a dedicated experimental campaign focused on fast electron physics and its interaction with turbulence, and it was optimised for extensive diagnostic coverage. As a result, most of the simulation input parameters—magnetic equilibrium, density and temperature profiles, loop voltage, effective charge Z_{eff}, and the spatial distribution of density and temperature fluctuations—are already well constrained. Since *LUKE* does not inherently model turbulent transport effects, an ad hoc radial transport term for suprathermal electrons is introduced to bring the simulation results into alignment with experimental observations. Optimising the functional form and amplitude of this transport term constitutes the main forward modelling task within the workflow. To this end, having synthetic diagnostics for direct comparison with experimental data is essential. In addition to estimating the plasma current $I_p - I_{BS}$ (where an external estimate of the bootstrap current is subtracted, since *LUKE* in its standard configuration does not include neoclassical effects) two further synthetic diagnostics are employed for the HXRS and VECE systems on TCV, as noted in the introduction. The geometries of both diagnostics are shown in the leftmost panels of Figure 2.

The wave propagation calculated by WKBeam, incorporating density fluctuations fitted to experimental data, is also shown in the same figure. Based on these results, $\langle \mathbb{D}^{\mathrm{RF}} \rangle$ is computed and passed to LUKE. Figure 3 presents the resulting current density profiles, along with synthetic diagnostic predictions from three consecutive simulations: first without any turbulent effects, then with beam broadening only, and finally with both beam broadening and radial transport. The photon temperature T_γ in these plots describes the hard X-ray energy spectrum and is fitted through $I_{HXR}/dE = A/E \cdot e^{-E/T_\gamma}$ for each channel. These fits underscore the importance of accounting for the interplay with turbulence. While beam broadening alone provides a modest improvement, the combined inclusion of broadening and radial transport clearly yields the best agreement. Consistent with findings reported in [4, 13], simultaneous fitting of all synthetic diagnostics within experimental error bars required a phase-space-dependent contribution to the radial diffusion coefficient, proportional to the quasilinear wave interaction. The general functional form used for the radial transport flux in this work is a purely diffusive contribution of the following form, where $D_{r0,ES}$ and $D_{r0,RF}$ are tuneable parameters of dimensions $[m^2/s]$:

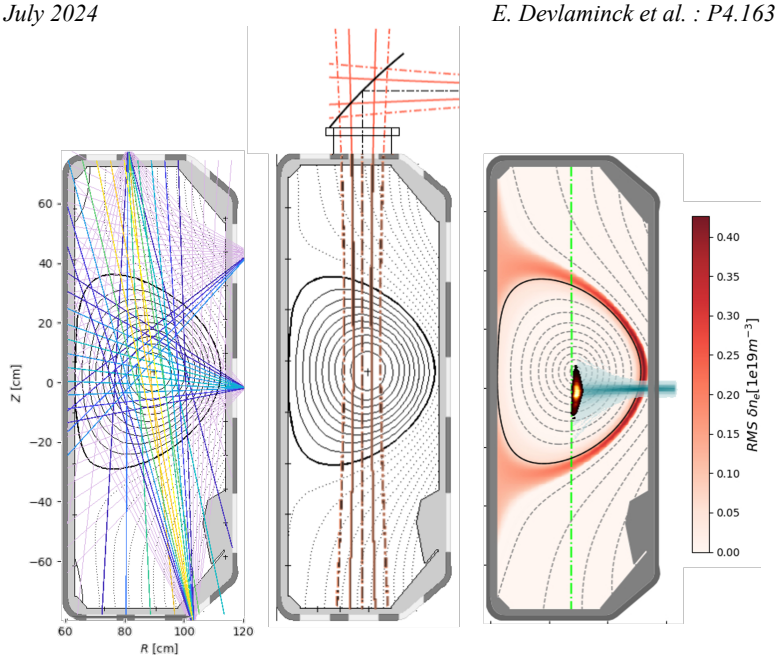

Fig. 2 *Left*: HXRS lines of sight on TCV. The channels used for analysis of TCV86148 are highlighted according to the measured intensity. *Middle*: VECE antenna pattern at $108.84GHz$ in vacuum. *Right*: Result of the *WKBeam* simulation including density fluctuations (*background red*), showing the wave propagation (*dark green*), absorption (*black-yellow*) and cold X2 resonance location (*green*). Spatial broadening is clearly noticeable.

$$\langle D_{rr} \rangle(\psi, p, \xi_0) = \left(D_{r0,ES}(1 + 3\psi^{3/2}) \frac{n_{e,0}}{n_e(\psi)} + D_{r0,RF} \langle \overline{D^{RF}} \rangle(\psi, p, \xi_0) \right) \cdot \mathcal{H}(p - p_{sup}) \quad (5)$$

In (5), $\mathcal{H}$ denotes the Heaviside function, which imposes a lower momentum threshold for suprathermal electron radial transport, with p_{sup} set to $3p_{th,0}$.

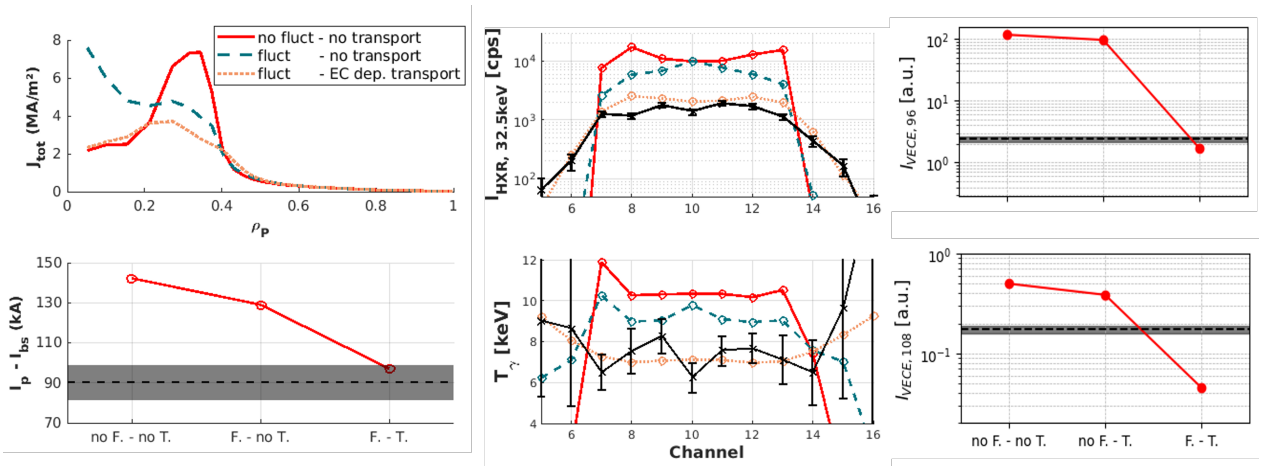

Fig. 3 Results for TCV86148, t=0.6s. Current density and total current (*left*), hard X-ray intensities and photon temperatures (*middle*) and VECE intensity predictions (*right*) all show satisfactory agreement with experimental values (*black, grey error bars*) only when density fluctuations and radial transport are taken into account.

The first term follows the radial dependence described in [3] for low-confinement (L-mode) plasmas, representing electrostatic 'background' turbulence. The second term captures the EC wave-dependent contribution, taken to be proportional to $\langle \overline{D^{RF}} \rangle$—the bounce-averaged quasilinear diffusion coefficient summed over all beams and harmonics, and normalised to its maximum value at the second harmonic. VECE predictions remain a point of concern in the current state of the workflow, but they are the subject of ongoing improvements, as the corresponding synthetic diagnostic was only recently re-implemented. The final electron distribution function, fitted radial diffusion coefficient and consequent radial electron flux are shown in Figure 4.

Conclusions

This work presents a suite of codes designed to address the long-standing challenge of reconciling FP simulations of tokamak experiments involving ECRH/ECCD with experimental observations. By accounting for both the scattering of the microwave beam by density fluctuations and turbulent radial transport of the subsequently created suprathermal electrons, multiple diagnostic predictions can be brought into agreement with the measurements upon the inclusion of a specifically tailored radial transport. Future work will focus on automating this tailoring process using Bayesian optimisation. A dedicated experimental campaign on TCV is also underway, aimed at characterising the required radial transport and mapping the associated particle fluxes and current drive. Finally, gyrokinetic simulations are envisioned to provide first-principles estimates of phase-space-resolved diffusion and convection. These could then be used to validate the present approach or serve directly as inputs to the workflow.

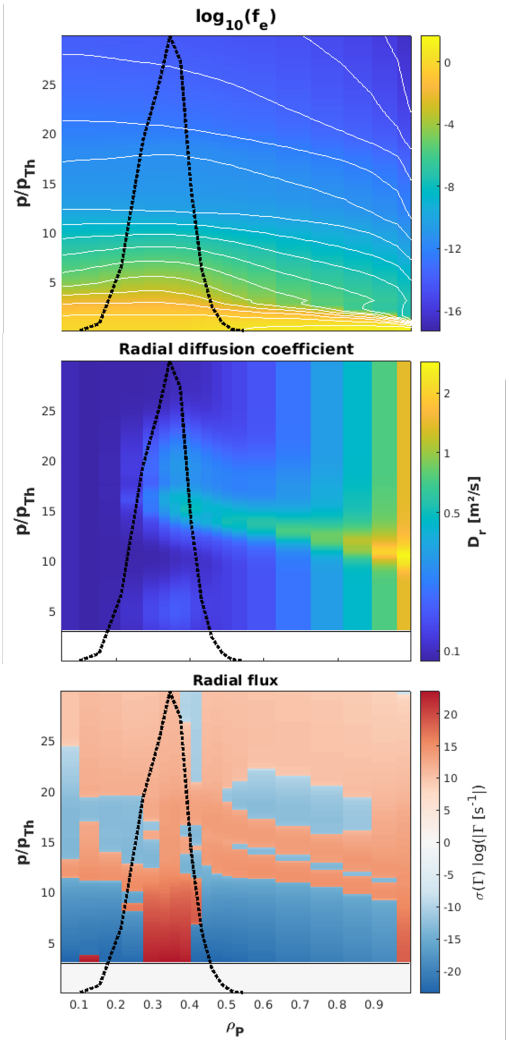

Fig. 4 *Top*: Resulting electron distribution function for TCV86148, t=0.6s. *Middle*: Fitted radial diffusion, with coefficients $D_{r0,ES} = 0.1$ and $D_{r0,RF} = 3.5[m^2/s]$ as in (5). *Bottom*: Radial electron flux through each flux surface $[\#e^-/s]$. Normalised $dP/d\rho$ is shown in *black*.

Acknowledgments

This work has been carried out within the framework of the EUROfusion Consortium, via the Euratom Research and Training Programme (Grant Agreement No 101052200 - EUROfusion) and funded by the Swiss State Secretariat for Education, Research and Innovation (SERI). Views and opinions expressed are however those of the author(s) only and do not necessarily reflect those of the European Union, the European Commission, or SERI. Neither the European Union nor the European Commission nor SERI can be held responsible for them. This work was supported in part by the Swiss National Science Foundation.

References

[1] I. T. E. R. Organisation. Technical Report ITR-18-003. ITER Organisation, 2018.
[2] S. Coda et al. *Nuclear fusion* 43.11 (2003), p. 1361.
[3] R. Harvey et al. *Physical review letters* 88.20 (2002), p. 205001.
[4] J. Cazabonne et al. *Plasma Physics and Controlled Fusion* 65.10 (2023), p. 104001.
[5] H. Weber. MA thesis. Max-Planck-Institut für Plasmaphysik, 2013.
[6] Y. Peysson and J. Decker. *Fusion Science and Technology* 65.1 (2014), pp. 22–42.
[7] Y. Peysson and J. Decker. *physics of plasmas* 15.9 (2008).
[8] L. Votta. MA thesis. Politecnico di Milano, 2021.
[9] J. Decker. PhD thesis. Massachusetts Institute of Technology, 2005.
[10] I. Lerche. *The Physics of Fluids* 11.8 (1968), pp. 1720–1727.
[11] C. Kennel and F. Engelmann. *Physics of Fluids* 9.12 (1966), p. 2377.
[12] Y. Peysson, J. Decker, and L. Morini. *Plasma Physics and Controlled Fusion* 54.4 (2012), p. 045003.
[13] D. Choi et al. *Plasma Physics and Controlled Fusion* 62.11 (2020), p. 115012.